

PACS numbers: 42.30.Wb; 42.40.Kw; 42.25.Dd; 42.25.Fx
DOI: 10.1070/QE2014v044n08ABEH015492

Improvement of lateral resolution of spectral domain optical coherence tomography images in out-of-focus regions with holographic data processing techniques

A.A. Moiseev, G.V. Gelikonov, D.A. Terpelov, P.A. Shilyagin, V.M. Gelikonov

Abstract. **An analogy between spectral-domain optical coherence tomography (SD OCT) data and broadband digital holography data is considered. Based on this analogy, a method for processing SD OCT data, which makes it possible to construct images with a lateral resolution in the whole investigated volume equal to the resolution in the in-focus region, is developed. Several issues concerning practical application of the proposed method are discussed.**

Keywords: *optical coherence tomography, digital holography.*

1. Introduction

Since the time when the possibility of using optical coherence tomography (OCT) to construct *in vivo* high-quality images of the internal structure of biological objects was experimentally demonstrated for the first time [1], the range of various applications of this method, which allows one to study noninvasively objects with a high spatial resolution (from several micrometres to several tens of micrometres), in research and clinical practice constantly increases. The method is based on the interference detection of light reflected or backscattered from internal inhomogeneities of the effective optical refractive index of a medium under study and measurement of its intensity. To date, several research teams from Europe, Asia, Russia and the United States have performed successful experiments aimed at improving OCT and implementing it in biomedical practice. The use of fibre OCT interferometers in optical schemes made it possible to apply these systems in endoscopic studies [2, 3] and, correspondingly, make the range of OCT applications wider.

A.A. Moiseev, D.A. Terpelov Institute of Applied Physics, Russian Academy of Sciences, ul. Ul'yanova 46, 603950 Nizhnii Novgorod, Russia; e-mail: aleksandr.moiseev@gmail.com, terpelov@ufp.appl.sci-nnov.ru;
G.V. Gelikonov, P.A. Shilyagin Institute of Applied Physics, Russian Academy of Sciences, ul. Ul'yanova 46, 603950 Nizhnii Novgorod, Russia; Nizhnii Novgorod State Medical Academy, pl. Minina i Pozharskogo 10/1, 603005 Nizhnii Novgorod, Russia; e-mail: grigory@ufp.appl.sci-nnov.ru; paulo-s@mail.ru;
V.M. Gelikonov Institute of Applied Physics, Russian Academy of Sciences, ul. Ul'yanova 46, 603950 Nizhnii Novgorod, Russia; Nizhnii Novgorod State Medical Academy, pl. Minina i Pozharskogo 10/1, 603005 Nizhnii Novgorod, Russia; N.I. Lobachevsky Nizhnii Novgorod State University, prosp. Gagarina 23, 603950 Nizhnii Novgorod, Russia; e-mail: gelikon@ufp.appl.sci-nnov.ru

Received 11 March 2014; revision received 26 June 2014
Kvantovaya Elektronika **44** (8) 732–739 (2014)
Translated by Yu.P. Sin'kov

One of the most important characteristic of an OCT system, as well as any other imaging systems, is its resolution. The axial and lateral resolutions in OCT (along and across a scanning beam) have different physical natures. The axial resolution is determined by the bandwidth (tuning range) of the light source used, while the lateral resolution is determined by the scanning-beam diffraction properties. The development of the physics of femtosecond laser sources provided an axial resolution better than 4 μm [4]. At the same time, the improvement of OCT lateral resolution is limited, because an increase in the probe-beam focusing sharpness reduces the depth of analysis because of the increased axial inhomogeneity of object illumination, which is caused by the scanning-beam diffraction divergence.

To date, there are several instrumental methods for improving the lateral OCT resolution with conservation of the analytical depth [5–7]. However, their implementation in the form of miniature endoscopic probes meets some technical difficulties, which hinder their use in endoscopic tools.

In recent years, researchers have been interested in the methods that make it possible to compensate for the influence of diffraction on the spatial resolution in OCT images in out-of-focus regions [8–10]. Despite the progress in this field, a number of problems related to the use of these methods in OCT systems remain to be solved. The purpose of this study was to develop a method for processing SD OCT data that is expected to improve the lateral resolution in out-of-focus regions to the level characteristic of the in-focus region.

2. Holographic approach to processing OCT data

This approach is based on the analogy (noted in [11]) between any two-dimensional sample (at certain values of wave numbers k), selected from an array of recordings of the interference field spectrum in the three-dimensional XYk space, obtained as a result of lateral scanning using a SD OCT system, and a digital hologram, recorded by a photodetector array. Indeed, a scattered field recorded by a SD OCT system can be written as

$$f_{\mathrm{OCT}}(x,y,k) = \int \mathrm{d}z g^2_{\mathrm{OCT}}(x,y,z,k) \otimes o(x,y,z), \qquad (1)$$

where $g_{\mathrm{OCT}}(x,y,z,k)$ is the scanning-beam field distribution at a distance z from the focal plane of the objective (this function is squared, because the same optical path is used to illuminate the object and receive the field scattered by it); $o(x,y,z)$ is the distribution of scatterers in the object under study; $\otimes$ is a convolution in the XY plane; and $k = 2\pi/\lambda$. Note that

$g_{\mathrm{OCT}}(x,y,z,k)$ is unambiguously determined at any distance from the focal plane as a convolution of the distribution in the focal plane and the kernel of propagation in free space. To make further calculations convenient, we will write the spectrum $f(x,y,z)$ in the form

$$\tilde{f}_{\mathrm{OCT}}(u,v,k) = \int \mathrm{d}z FT_{x,y\to u,v} g^2_{\mathrm{OCT}}(x,y,z,k)\,\tilde{o}(u,v,z)$$

$$= \int dz \left\{ \left[\tilde{g}_{\mathrm{OCT}}(u,v,z_0,k) \exp\left(\mathrm{i}kz - \mathrm{i}\frac{u^2+v^2}{2k}\Delta z \right) \right] \right.$$

$$\left. \otimes \left[\tilde{g}_{\mathrm{OCT}}(u,v,z_0,k) \exp\left(\mathrm{i}kz - \mathrm{i}\frac{u^2+v^2}{2k}\Delta z \right) \right] \right\} \tilde{o}(u,v,z). \quad (2)$$

Here, the tilde sign indicates that a function (or operator) belongs to the Fourier-space; the transfer function of free space is written in the small-angle approximation ($u^2 + v^2 \ll k^2$) [12]; u and v are the values of lateral wave vectors in the Fourier space; z_0 is the position of the focal plane; and $\mathrm{FT}_{x,y\to u,v}$ is a direct Fourier transform. For simplicity, we assume the scanning beam to have a Gaussian distribution. In this case, the field distribution in the focal plane of the objective, $g_{\mathrm{OCT}}(x,y,z,k)$, as well as its spectrum, is also Gaussian. Thus, we can write

$$\tilde{f}_{\mathrm{OCT}}(u,v,k) = \int \mathrm{d}z \exp\left(2\mathrm{i}k\Delta z - \mathrm{i}\frac{u^2+v^2}{4k}\Delta z \right)$$

$$\times \exp\left(-\frac{u^2+v^2}{2} W_0^2 \right) \tilde{o}(u,v,z). \quad (3)$$

Here, $W_0 = \pi/(\mathrm{NA}k)$ is size of the scanning beam waist and NA is the numerical aperture of the objective (we used an objective with NA = 0.1 to avoid the problems related to the use of the small-angle approximation in systems with a large numerical aperture [13]).

The equation describing the spectrum of a broadband lensless digital holography signal has the form [14]

$$\tilde{f}_{\mathrm{BDH}}(u,v,k) = \int \mathrm{d}z \exp\left(2\mathrm{i}k\Delta z - \mathrm{i}\frac{u^2+v^2}{2k}\Delta z \right) \tilde{o}_{\mathrm{I}}(u,v,z). \quad (4)$$

A comparison of Eqns (3) and (4) shows that the SD OCT signal coincides exactly with the lensless digital holography signal for an object having the distribution

$$o_{\mathrm{I}}(x,y,z) = o(x,y,z) \otimes \exp\left(-\frac{x^2+y^2}{W_0^2} \right)$$

with a change in the values of lateral wave vectors u and v by a factor of $\sqrt{2}$.

An important feature of the point-to-point recording of an interference pattern is the influence of the confocal character of probing in an OCT system, which leads to a decrease in the total signal from each point scatterer with an increase in the distance from the focal plane. In addition, as was indicated above, this signal is distributed in the XY plane because of diffraction. The methods described in this study make it possible to compensate for the influence of diffraction; however, they cannot prevent the attenuation of the total signal with an increase in the distance from the focal plane. Nevertheless, this circumstance allows one to use more efficiently the OCT dynamic range by choosing correctly the initial position of the focal plane in the bulk of the object under study. In this case, the signal attenuation with increasing depth will be partially compensated for by an increase in the radiation density when approaching the focal plane.

The analogy between the SD OCT and broadband holography signals makes it possible to process these signals by holographic methods. We used the method of expanding SD OCT in plane waves [12] to construct a scattered-field distribution at each wavelength of the spectral expansion of source radiation. This method is based on the representation of the field in the XY plane (which is perpendicular to the field propagation direction Z) in the form of a superposition of plane waves propagating at different angles. The field in the plane at a distance Z from the initial plane is a superposition of the plane waves forming the initial distribution and transferred at the same distance. When propagating, a plane wave acquires an additional phase $\mathrm{i}k_z Z$, where k_z is the wave-vector component in the propagation direction. Thus, one can calculate field distributions at any distance z from the initial plane by multiplying the two-dimensional spectrum of the field in the initial XY plane ($z = 0$) by the corresponding phase mask, with a subsequent inverse Fourier transform. Note that this way for solving the diffraction problem allows one to calculate a field at any distance z from the initial XY plane ($z = 0$); in addition, it is computationally efficient because involves only two Fourier transforms and one multiplication.

The scattered-field distribution at one component of the source-radiation spectral expansion has the form

$$f(x,y,z,k) = \mathrm{iFT}_{u,v\to x,y}$$

$$\times \left\{ \mathrm{FT}_{x,y\to u,v}(f(x,y,0,k)) \exp\left[\mathrm{i}kz - \mathrm{i}\frac{u^2+v^2}{4k} z \right] \right\}, \quad (5)$$

where $f(x,y,0,k)$ and $f(x,y,z,k)$ are the field distributions in the focal plane and at an optical distance Δz from it and $\mathrm{iFT}_{u,v\to x,y}$ is the inverse Fourier transform in the plane perpendicular to the scanning-beam direction. When a field propagates at corresponding distances z, one can reconstruct the scattered-field distribution in the whole volume under study at each k. The field at one wavelength yields a pattern of the scatterer distribution in the object studied; the resolution throughout the entire volume is determined by the scanning-beam diffraction properties. As in the case of broadband digital holography, one must sum field distributions at all wavelengths, so as to make the axial resolution be determined by the source radiation bandwidth [15]:

$$F(x,y,z) = \sum_k \mathrm{iFT}_{u,v\to x,y} \left[\mathrm{FT}_{x,y\to u,v}(f(x,y,0,k)) \right.$$

$$\left. \times \exp\left(\mathrm{i}kz - \mathrm{i}\frac{u^2+v^2}{4k} z \right) \right]. \quad (6)$$

Equation (6) makes it possible to obtain an image with a lateral resolution equal to the resolution in the scanning-beam focal plane, whereas the axial resolution is determined by the spectral properties of the source radiation.

Note that one can reconstruct an image in the entire volume studied using direct calculations based on formula (6) only when the initial position of the focal plane and the refractive index of the medium under study are known. Note that the ratio of the distances between scatterers along the Z axis in an OCT image is proportional to the ratio of the optical

distances between these scatterers in space. In view of this, one can consider the refractive index rather than the refractive index distribution in the medium as a parameter. Figure 1b shows a numerically reconstructed image of scatterers according to formula (6) over the entire XZ plane in the case of tight beam focusing for experimentally obtained OCT images of point scatterers (abrasive powder with a grain size of 10 μm), spatially fixed in a homogeneous medium (transparent photo glue). When these parameters differ from optimal by 10%, a calculation based on formula (6) does not yield the desired result (Fig. 1c). To estimate the efficiency of the proposed methods for improving the lateral resolution of images, the dependences of the point-scatterer characteristic width on depth were investigated for experimental data. Although this width depends on not only the lateral resolution of the system but also on the scatterer characteristic size, the proposed approach allows one to compare the resolution before and after applying the methods under consideration. Since the resolution of the OCT system in the probe focal region is known (it is determined by the numerical aperture of the objective), a comparison of the characteristic width of a point scatterer with its width in the focal region of the initial distribution makes it possible to estimate the resolution of the system throughout the entire depth. Figures 1b, 1c and 1d show that the OCT image resolution obtained using formula (6) at optimal parameters, at a distance from the focal region on the order of five Rayleigh lengths, corresponds to the resolution of the initial image in the focal region. This resolution is ~6 μm in air (for a wavelength of 1.3 μm and objective numerical aperture of 0.1). At the same time, if the algorithm parameters differ from optimal by 10%, the diffraction spread at a significant distance from the focal plane is incompletely compensated for, despite the increased focus depth in this image.

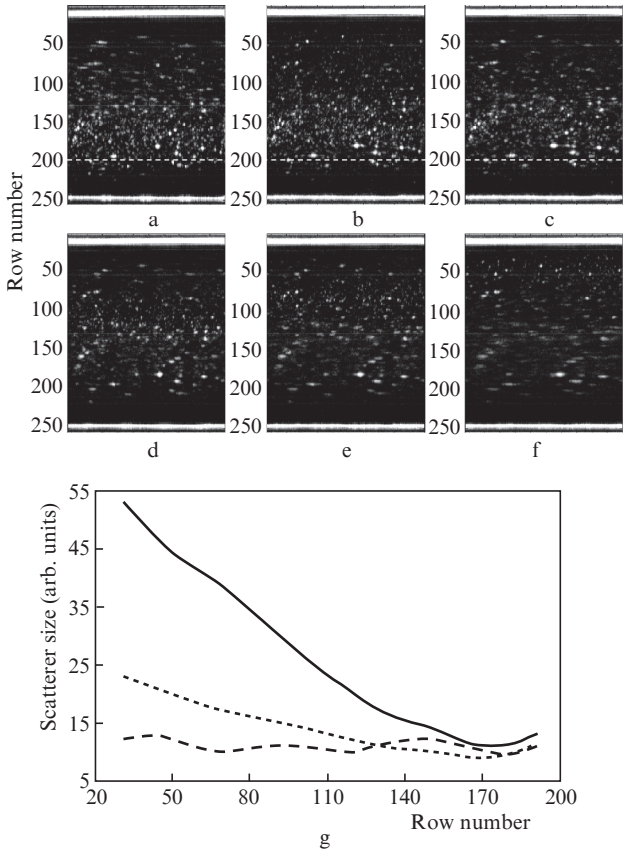

Figure 1. Image of an array of point scatterers in a homogeneous medium, obtained by scanning a sample with a tightly focused beam using (a) conventional data processing, (b) processing data according to formula (6) with optimal values of algorithm parameters, (c) processing data according to formula (6) with values of algorithm parameters differing from optimal by 10%, and (d–f) after numerical transfer of the focal region according to formula (7). The images in panels (d) and (f) were obtained for refractive indices differing by ±20% from the value specified for the image in panel (e). Panel (g) shows the characteristic width of point scatterers in the images in panels (a) (solid line), (b) (dashed line) and (c) (dotted line). The dashed lines in panels (a–c) indicate approximately the initial position of the focal plane.

We proposed a method for determining the parameters that are necessary for constructing OCT images with a resolution throughout the entire depth under study equal to the resolution in the focal plane. Note that for each specific Δz value the results of calculations based on formula (6) exactly coincide with the results obtained using the formula

$$F_1(x,y,z,\Delta z) = \sum_k \exp(ikz)\,\mathrm{iFT}_{u,v\to x,y} \times\left[\mathrm{FT}_{x,y\to u,v}(f(x,y,0,k))\exp\left(-i\Delta z\frac{u^2+v^2}{4k}\right)\right]. \qquad (7)$$

This operation shifts the image focal region by a distance Δz (Fig. 1e). If the parameters specified in the algorithm based on formula (7) differ from optimal, the focal region also shifts by the corresponding optical distance; however, the position of this region in the OCT image is not determined beforehand (Figs 1d, 1f).

Taking into account that (i) at any deviation of the refractive index of a medium under study and its value specified in calculations from the actual value the calculations based on formula (7) lead to a numerical transfer of the OCT image focus and (ii) the refractive indices of media studied by OCT lie in some range, one can construct a procedure similar to the procedure of synthesizing a high-resolution image from a series of images focused at different depths, which is used in optical coherence microscopy [5, 6]. To this end, it is necessary to transfer numerically the focal plane of the initial image by several (specified beforehand) Δz values. The shifts must be such as to make the focal regions of images with numerically transferred foci overlap at any refractive index that a biological medium may have. Actually, this means that this overlap should be observed at a minimally possible refractive index.

At the same time, according to the results of the numerical focus transfer, one can determine the optical distances corresponding to the distances in the image and find the initial position of the focal plane and then use these data to calculate OCT images with improved lateral resolution from formula (6).

Indeed, calculations based on formula (7) at some values of the wave-vector lateral components u and v imply multiplication of the initial vector by the matrix

$$M_{nm} = \exp\left[i\frac{2\pi mn}{N} + \alpha(N_i - N_0)\frac{(\Delta up)^2 + (\Delta vl)^2}{4(k_{\min} + \Delta km)}\right], \qquad (8)$$

where p and l are the lateral indices of the angular spectrum; Δu and Δv are the sampling parameters of the angular spectrum $u = \Delta up$ and $v = \Delta vl$); N is the number of spectral references; $k_{\min} = 2\pi n_r/\lambda_{\max}$; $\Delta k = (2\pi n_r/\lambda_{\min} - 2\pi n_r/\lambda_{\max})/N$; $\lambda_{\min}$ and

λ_{max} are, respectively, the minimum and maximum wavelengths in the source radiation spectrum; m is the index in the wave-number space; $z = \alpha(N_i - N_0)$; N_0 is the initial position of the focal plane; α is the optical distance between neighboring planes (enumerated by index n in the image space); and αN_i determines the Δz_i value (the optical path at which the focal plane must be transferred). Note again that the dependence $z(n)$ remains linear at any distribution of the refractive index n_r, because the measured modulation of the optical spectrum of OCT interference signal is determined by the phase intervals (controlled by the optical length). Calculations with the aid of matrix (8) imply multiplication of a three-dimensional spectrum by a phase mask with a subsequent Fourier transform over equidistantly sampled references. Note also that, having replaced the N_i value in formula (8) with a variable n, we obtain coefficients of the matrix used to carry out transform (6).

Let us consider the problem of determining parameters α and N_0. Let them be set so that, at their substitution into formula (6) for calculating the distribution with improved lateral resolution, the resolution throughout the entire object depth corresponds to the in-focus resolution. Then the focal plane in the image calculated from formulas (7) and (8) will be numerically transferred onto the N_i plane. If parameters α_1 and N_1 differing from α and N_0 are set, the focal plane will be transferred onto the N_j plane with an index satisfying the condition $\alpha_1(N_j - N_1) = \alpha(N_i - N_0)$. If an analysis of the image allows one to find the position of the focal plane both in the initial image (N_0) and in the images obtained after numerical focus transfer (N_j), the desired dependence can be found by calculating the parameter α.

Unfortunately, the exact position of the focal plane is not determined even in an image of a relatively simple model object (point scatterers in a homogeneous medium). In the case of a biological object, which does not have a certain geometric structure, the situation is even more difficult. Note also that it is impossible to introduce some objective (numerical) parameter determining the focal plane, because distributions at different depths may significantly differ, and the difference in the numerical parameters will be caused by the specific features of the object studied rather than the quality of the OCT image obtained at a particular depth. Thus, both parameters, α and N_0, must be determined.

To find the parameters of the linear dependence $\alpha(N_i - N_0)$, we must determine the optical distance from the initial focal plane to any two of N XY planes in the image. To this end, we will 'refocus' the initial data to two depths and search for the XY plane located in the middle of the optical distance between the initial and numerically transferred focal planes for each image obtained. From the physical point of view, at a given optical depth, the curvature of the parabolic phase mask in the UV Fourier space, which causes diffraction blurring of images, will change sign, while the spectral widths of the spatial distributions of the scattered-wave amplitude in the XY plane in the initial image and in the image with a numerically transferred focus should coincide (Fig. 2a). From the computational point of view, it is expedient to replace the procedure of comparing the phase-mask curvature in the UV Fourier space for each distribution in the XY plane by a procedure of comparing the spatial spectrum width for the distributions of scattered-wave amplitude in the XY plane in the initial image and in the image with a numerically transferred focus. The spectral width was determined at a level

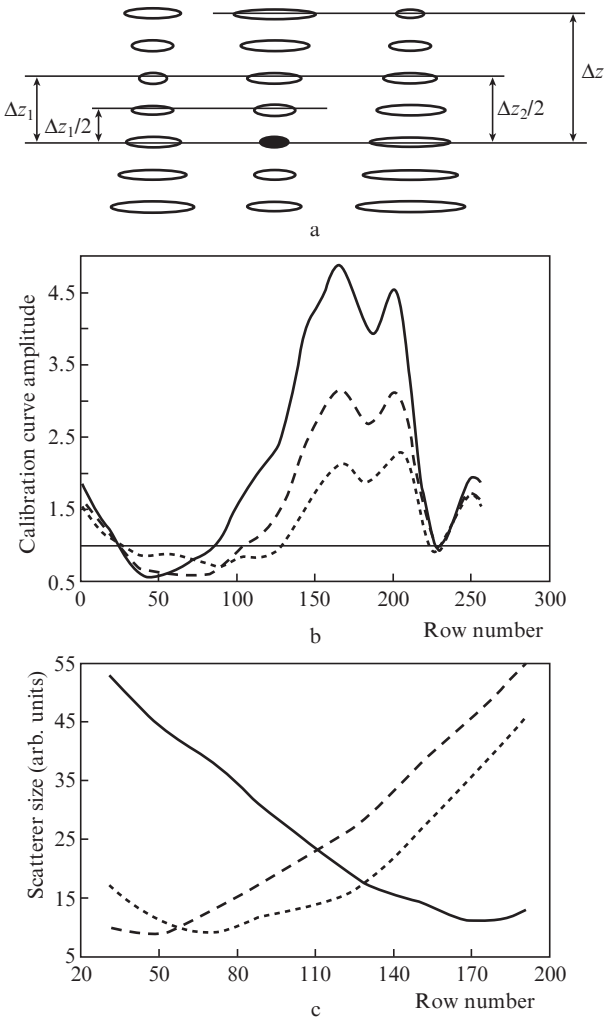

Figure 2. (a) Initial image (in the centre); the initial focus position is indicated by a filled ellipse, the images on the right and on the left are obtained by transferring the focal region by Δz_1 and Δz_2, respectively; the characteristic width of the scattering function of a point object remains invariable at distances $\Delta z_1/2$ and $\Delta z_2/2$, respectively. (b) The calibration curves, obtained for point scatterers in a homogeneous medium by numerical transfer of focus at three different depths. (c) The dependence of the point-scatterer characteristic width on depth for the initial image (solid line) and the images with a numerically transferred focus (dashed and dotted lines).

of 70% of the spectral component with maximal amplitude.

Thus, to determine the plane in which the phase-front curvature changes its sign, we plotted a dependence of the initial-image spectral width on the spectral width of the image with a numerically transferred focus. The thus obtained curve was passed through a low-pass filter to eliminate the influence of noise, and its intersection with the level of unity was sought for. The coordinates of this intersection correspond to the desired position $N_{j1/2}$ (Fig. 2b). As a result, each focus transfer can be described by the equation

$$2\alpha(N_{j1/2} - N_0) = \Delta z_j. \tag{9}$$

At a specified Δz_j value, we determine $N_{j1/2}$ in the above-described way. Thus, we have a system of linear equations as a base for finding parameters α and N_0, which are necessary for both the controlled numerical transfer of the focal plane

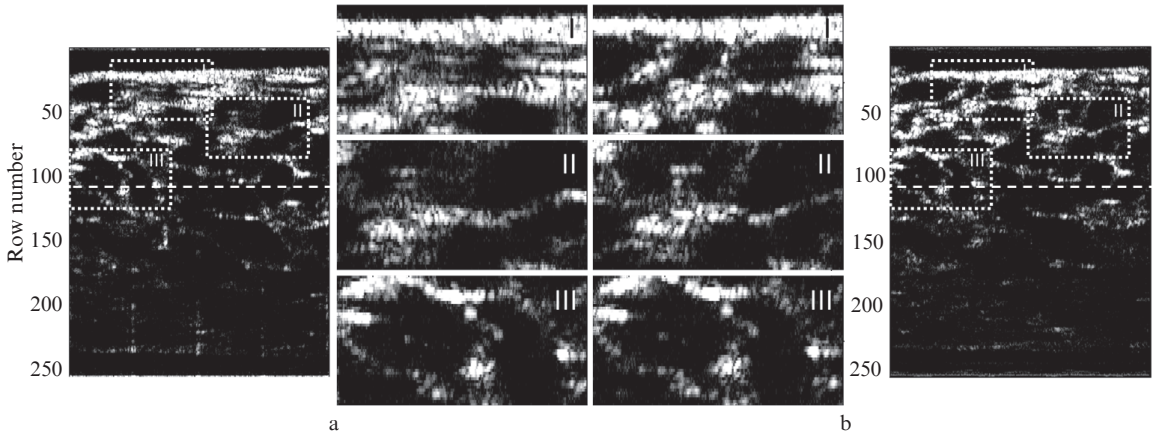

Figure 3. (a) Initial image of orange pulp and (b) an image obtained from formula (6); (I–III) enlarged portions of the images in panels (a) and (b) at different distances from the initial focal plane; the dashed lines indicate approximately the initial position of the focal plane.

and for calculations based on formula (6). This transform can be calculated as a discrete Fourier transform over nonequidistantly sampled data. Although the implementation of this transform using a fast Fourier transform gives rise to significant artefacts [whereas $O(N^2)$ operations are necessary for its exact calculation], there are many schemes for its approximate calculation [16–18].

Note that, with allowance for the determination of the algorithm parameters, to reconstruct an OCT image with a resolution throughout the entire volume under study corresponding to the in-focus resolution, it is necessary to transfer numerically the focal plane two times, find the dependence $\Delta z(N_i)$, and perform a calculation based on formula (6).

The resolution of the images obtained was determined by estimating images of an object in the form of a point-scatterer array in a homogeneous medium (i.e., an object similar to that described above). It was established that the resolution throughout the volume under study corresponds to the in-focus resolution of the initial images.

The above-considered method was also tested on biological objects. Figure 3a shows a distribution obtained by conventional processing SD OCT data, and Fig. 3b presents an image produced by reconstructing the resolution corresponding to the in-focus resolution in the volume under study using the parameters found with the aid of the proposed technique. Regions I–III, located at different distances from the initial focal plane, are selected in the images. It can be seen that images near the surface (beyond the focal region) became sharper in Fig. 3b, whereas the images near the initial focal plane barely changed. As a result, the image in Fig. 3b demonstrates the same resolution throughout the entire depth studied; the lateral resolution near the surface (in the out-of-focus region) is improved.

3. Determination and compensation for the two-dimensional distribution of phase instability

The decisive factor affecting the applicability of the above-described methods to real-data arrays is the phase stability, i.e., the constancy of the distance between the reference shoulder and the object during recording each array element. Note that phase stability is called for not only in the applications aimed at improving the resolution in out-of-focus regions of OCT images but also in Doppler OCT [19], phase microscopy [20], polarisation-sensitive OCT [21], coherent averaging [22] and spectroscopic OCT [23]. The use of SD OCT with a spectrometer for recording data allows one to retain the phase constancy at each lateral position of scanner, because data distributions over the wave number are recorded simultaneously at all k values. Unfortunately, various thermal effects, errors in positioning the scanner or reference mirror and object motions [24] may cause phase instability during lateral scanning. A variation in the distance between the reference shoulder and object by λ leads to addition of a scattered field with a phase 2π to the corresponding lateral reference measured by the OCT system. Such small motions can hardly be observed in the conventionally obtained SD OCT images [25]; however, they are destructive for all methods manipulating with the OCT data phase. Generally, a surface obviously immobile with respect to the object was generally used to obtain phase stability [20, 26]. This approach leads to a corresponding complication of the system, and its joint implementation with an endoscopic probe is a technically complex problem.

A measurement of the interference field scattered by an object and the reference-wave field at different positions of the reference shoulder provides the value of scattered-wave complex field in each lateral position of the scanner [27, 28]. Therefore, we will deal with a complex value of a field scattered by an object in this section. To determine and compensate for the phase error, it would be of interest to find the phase difference between two neighbouring lateral measurements of the signal spectrum in the SD OCT. This value can be estimated by operating with the quadrature components of the neighbouring distributions of signal spectrum (i.e., with the real part of one distribution and the imaginary part of a neighbouring one). We assume that neighbouring lateral measurements of signal spectrum were made rather closely (with the Kotel'nikov–Nyquist criterion satisfied) and that there is a spurious phase difference between them. The quadrature components of neighbouring distributions of the optical spectrum obey the following relations:

$$C_{i,j} = \mathrm{Re}[f(x,y,0,k)\exp(\mathrm{i}\Phi_{i,j})],$$
$$S_{i,j+1} = \mathrm{Im}[f(x,y,0,k)\exp(\mathrm{i}\Phi_{i,j+1})] \qquad (10)$$

$$= \mathrm{Im}\{f(x,y,0,k)\exp[\mathrm{i}(\Phi_{i,j} + \Delta\Phi_{i,j+1/2})]\} =$$

$$= \sin\Delta\Phi_{i,j+1/2}\,\mathrm{Re}[f(x,y,0,k)\exp(\mathrm{i}\Phi_{i,j})]$$

$$+ \cos\Delta\Phi_{i,j+1/2}\mathrm{Im}[f(x,y,0,k)\exp(\mathrm{i}\Phi_{i,j})],$$

where $f(x,y,0,k)$ is a complex signal, manipulations with which allow one to perform numerical refocusing without distortions; $\Phi_{i,j}$ is the phase error, which must be found and compensated for; and $\Delta\Phi_{i,j+1/2}$ is the phase difference for references with indices i,j and $i,j+1$. If arrays $C_{i,j}$ and $S_{i,j+1}$ are sufficiently large and a signal from many scatterers is observed, one can expect the inequality

$$\sum\{\mathrm{Re}[f(x,y,0,k)\exp(\mathrm{i}\Phi_{i,j})]\}^2$$

$$\gg \sum\mathrm{Re}[f(x,y,0,k)\exp(\mathrm{i}\Phi_{i,j})]\mathrm{Im}[f(x,y,0,k)\exp(\mathrm{i}\Phi_{i,j})]$$

to be satisfied. Here, summation is over array elements and multiplication is performed elementwise. Indeed, the left-hand side of this inequality is a sum of nonnegative terms, whereas the right-hand side is a sum of alternating terms. The intermediate (with respect to k) values of magnitudes $|\mathrm{Re}[f(x,y,0,k)\exp(\mathrm{i}\Phi_{i,j})]|$ and $|\mathrm{Im}[f(x,y,0,k)\exp(\mathrm{i}\Phi_{i,j})]|$ are comparable. The phase difference of horizontally neighbouring lateral measurements of signal spectrum in SD OCT is determined as

$$\Delta\Phi_{i,j+1/2} = \arcsin\left[\frac{\sum\limits_k C_{i,j}S_{i,j+1}}{\sum\limits_k C_{i,j}^2}\right],$$

$$\cos\Delta\Phi_{i,j+1/2} = \pm\sqrt{1 - \left(\frac{\sum\limits_k C_{i,j}S_{i,j+1}}{\sum\limits_k C_{i,j}^2}\right)^2}, \qquad (11)$$

$$S'_{i,j+1/2} = \left(S_{i,j+1} - C_{i,j}\frac{\sum\limits_k C_{i,j}S_{i,j+1}}{\sum\limits_k C_{i,j}^2}\right)(\cos\Delta\Phi_{i,j+1/2})^{-1}.$$

The correct sign at $\cos\Delta\Phi_{i,j+1/2}$ can be chosen from the position of the boundary in the depth distribution of scatterers obtained as a result of the Fourier transform of a complex signal composed of $C_{i,j+1}$ and $S'_{i,j}$, after which $\Delta\Phi_{i,j+1/2}$ can be found in the range from $-\pi$ to π. Similarly, one can find $\Delta\Phi_{i+1/2,j}$ (the phase difference between two neighbouring distributions of optical spectrum in the vertical direction). Thus, the phase error gradient $\Phi'(x,y)$ can be determined and used to find the phase error. Based on the information about field gradients, one can write the following system of equations for determining the phase error:

$$\Phi'_{i,j+1} - \Phi'_{i,j} = \Delta\Phi_{i,j+1/2}\ (i = 0,\ldots,N-1, j = 0,\ldots,N-2),$$

$$\Phi'_{i+1,j} - \Phi'_{i,j} = \Delta\Phi_{i+1/2,j}\ (i = 0,\ldots,N-2, j = 0,\ldots,N-1). \qquad (12)$$

Here, $\Phi'_{i,j}$ is the estimated the phase error; this estimation is obtained from the field of phase error gradients, calculated according to formulas (11). The system of equations (12) is overdetermined and can be solved by any method allowing one to estimate a solution to a system of linear equations in the sense of least rms error. It was shown in [29] that the solution minimising the functional

$$\sum_{i=0}^{N-2}\sum_{j=0}^{N-1}(\Phi'_{i+1,j} - \Phi'_{i,j} - \Delta\Phi_{i+1/2,j})^2$$

$$+ \sum_{i=0}^{N-1}\sum_{j=0}^{N-2}(\Phi'_{i,j+1} - \Phi'_{i,j} - \Delta\Phi_{i,j+1/2})^2 \qquad (13)$$

is a solution to the equation

$$a_i(\Phi'_{i+1,j} - \Phi'_{i,j}) - a_{i-1}(\Phi'_{i,j} - \Phi'_{i-1,j}) + b_j(\Phi'_{i,j+1} - \Phi'_{i,j})$$

$$- b_{j-1}(\Phi'_{i,j} - \Phi'_{i,j-1}) = a_i\Delta\Phi_{i+1/2,j} - a_{i-1}\Delta\Phi_{i-1/2,j}$$

$$+ b_j\Delta\Phi_{i,j+1/2} - b_{j-1}\Delta\Phi_{i,j-1/2}, \qquad (14)$$

where $i,j = 0,\ldots,N-1$; $a_i = 1$; $i = 0,\ldots,N-2$; $a_{-1} = a_{N-1} = 0$; $b_j = 1$; $j = 0,\ldots,N-2$; and $b_{-1} = b_{N-1} = 0$.

Equation (14) is a discrete version of the Poisson equation with boundary Neumann conditions [29]:

$$\frac{\partial^2\Phi'}{\partial x^2} + \frac{\partial^2\Phi'}{\partial y^2} = \nabla\cdot\boldsymbol{s}. \qquad (15)$$

Here, Φ' is the desired estimate of phase distribution and $\boldsymbol{s}$ is the experimental distribution of the field of phase error gradients obtained from formulas (11). Field $\boldsymbol{s}$ can presented as a superposition of the gradient of some distribution Φ' and the solenoidal part of $\boldsymbol{s}_R$ (i.e., the part that cannot be presented as a gradient of distribution). The solution to Eqn (14) is the distribution Φ' [30]. According to [30], $\boldsymbol{s}_R$ can be considered as the noise part of measurements. If this is an isotropic stationary Gaussian noise with a zero mean, Φ' is an estimate obtained by the maximum likelihood method (actually, under the aforementioned conditions on the additive noise, the estimates obtained by the least-squares method and the maximum likelihood method coincide). In the opposite case, as was shown in [30], the estimate found by the least-squares method yields an underestimated slope for the phase distribution.

Thus, using the gradient estimates provided by formula (11), one can estimate the desired two-dimensional phase-error distribution. The compensation for this error is reduced to multiplication of the initial data array by the corresponding phase mask:

$$f_\mathrm{r}(x,y,0,k) = f(x,y,0,k)\exp(-\mathrm{i}\Phi'_{i,j}). \qquad (16)$$

However, one cannot reconstruct the phase error profile by this method if the gradient field estimated from formula (11) contains a solenoidal part, the statistical properties of which do not satisfy the coincidence conditions for the estimates obtained by the maximum likelihood and least-squares methods. The probability of this situation is fairly high under real conditions. In this study, we propose a way for determining and compensating for the profile of this phase error. This process, described by Eqns (10)–(16), was applied to the data array $f_\mathrm{r}(x,y,0,k)$ and cyclically repeated:

$$f_{r(t)}(x,y,0,k) = f_{r(t-1)}(x,y,0,k)\exp(-i\Phi_{i,j}^{(t)}). \quad (17)$$

Here, t is the iteration number. The iteration process is continued until the maximum phase gradient $\Phi^{(t)}$ calculated at a current iteration becomes smaller than some specified threshold value. Note that this condition is finally satisfied because of the 'underestimated phase slope', which was indicated in [30]. The total phase error is determined as the sum of the phase errors found in all iterations. The desired complex signal, manipulations with which allow one to perform numerical refocusing without distortions, is $f_{r(Niter)}$.

The method proposed was tested on numerically simulated and experimental OCT data. The object of study was a simulated lateral distribution of scatterers with a pronounced structure (a number of bands in one of the directions), which simplified visual estimation of the method efficiency. The OCT data were calculated from the initial distribution of scatterers according to the results of [8]. To estimate the efficiency of the proposed method of compensating for the phase instability and demonstrate its effect on the possibility of compensating for the influence of diffraction, we calculated in each case the overlap integral of the field distribution obtained after an attempt to compensate for diffraction (Figs 4c, 4e, 4f, 4h, 4i) with the initial field distribution (Fig. 4a). The overlap integral was calculated from the formula

$$\eta = \frac{\sum F_{init} F^*_{refoc} \sum F^*_{init} F_{refoc}}{\sum |F_{init}|^2 \sum |F_{refoc}|^2}. \quad (18)$$

Here, F_{init} and F_{refoc} are, respectively, the initial and final field distributions and the asterisk sign indicates complex conjugation; summation is over all distributions. The results of the corresponding calculations are given in the caption to Fig. 4. When comparing the value of this coefficient before and after applying the algorithm for finding and compensating for the phase error, one can note its efficiency even at a random change in the phase between lateral measurements of the interference signal spectrum in SD OCT.

The experimental study was also performed on an object with a pronounced structure: a deposited graduated scale oriented perpendicular to the scanning-beam optical axis. The phase error was due to vibrations occurring during scanning. The experimental results are shown in Figs 4j–4m. These vibrations manifest themselves as follows: the continuous bands obtained as a result of numerical transfer of the scale image appear uneven and intermittent (Fig. 4k), whereas few (specifically, five) iterations of the proposed algorithm provide a more reliable image of the test object (Fig. 4m). This experiment also makes it possible to estimate the resolution of the used OCT system, because the distance between neighbouring scale lines is known (10 μm), and these lines are completely resolved.

Thus, based on the analogy between the SD OCT and broadband digital holography data, we described a method for processing SD OCT data, which provides images with a lateral resolution throughout the entire volume under study corresponding to the resolution in the in-focus region. A technique for determining the parameters (dependent on the medium studied) that are necessary for efficient application of the proposed methods was developed. The problem of phase stability between lateral measurements in SD OCT was considered and a way of compensating for possible phase instability was proposed.

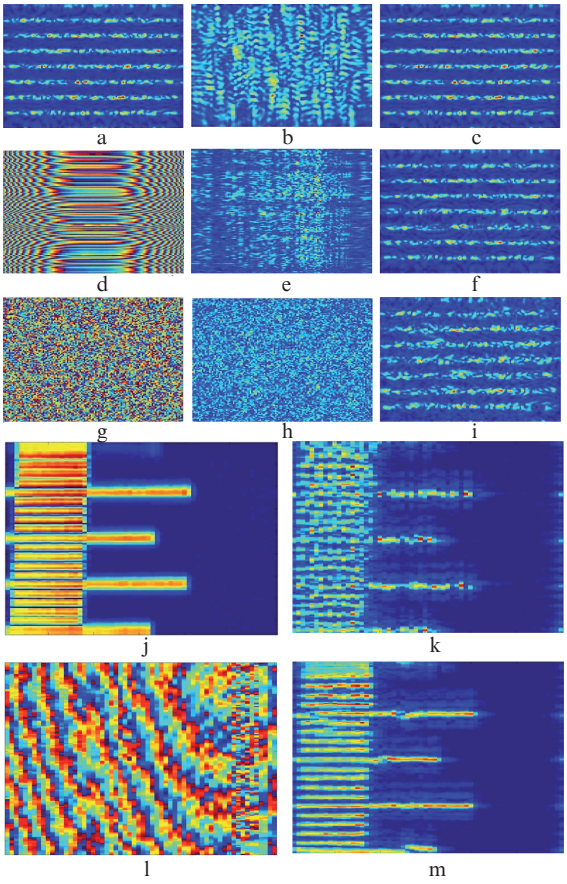

Figure 4. Numerical experiment on the operation of the phase equalisation algorithm: (a) test object (one plane in the volume, oriented perpendicular to the scanning beam); (b) defocused OCT image of the object (plane oriented perpendicular to the scanning beam); (c) result of numerical focus transfer in the absence of the phase error ($\eta = 0.98$); (d) simulated phase error, which is 'smooth' in the horizontal direction and has random discontinuities in the vertical direction; (e) an attempt to refocus OCT data with this error ($\eta = 0.12$); (f) an attempt to refocus OCT data with this error after 10 iterations of the phase equalisation algorithm ($\eta = 0.89$); (g) random phase error; (h) attempt to refocus OCT data with this error ($\eta = 0.06$); and (i) attempt to refocus OCT data with this error after 50 iterations of the phase equalisation algorithm ($\eta = 0.78$). The experimental results of phase equalisation: (j) initial object image in the plane perpendicular to the scanning beam, (k) attempt of numerical refocusing without additional processing, (m) attempt of refocusing after using the phase equalisation algorithm and (l) calculated phase error.

Acknowledgements. This work was supported by the Ministry of Education and Science of the Russian Federation (Contract No. 14.V25.31.0015, June 26, 2013) and the Russian Foundation for Basic Research (Grant No. 12-02-01160-a).

References

1. Swanson E.A., Izatt J.A., Hee M.R., Huang D., Lin C.P., Schuman J.S., Puliafito C.A., Fujimoto J.G. *Opt. Lett.*, **18** (21), 1864 (1993).
2. Sergeev A.M., Gelikonov V.M., Gelikonov G.V., Feldchtein F., Kuranov R., Gladkova N.D., Shakhova N.M., Snopova L., Shakhov A., Kuznetzova I., Denisenko A., Pochinko V., Chumakov Y., Streltzova O. *Opt. Express*, **1** (13), 432 (1997).
3. Tearney G.J., Brezinski M.E., Bouma B.E., Boppart S.A., Pitris C., Southern J.F., Fujimoto J.G. *Science*, **276** (5321), 2037 (1997).

4. Bourquin S., Aguirre A., Hartl I., Hsiung P., Ko T., Fujimoto J.G., Kopf D. *Opt. Express*, **11** (24), 3290 (2003).
5. Gelikonov G.V., Gelikonov V.M., Ksenofontov S.U., Morosov A.N., Myakov A.V., Potapov Y.P., Saposhnikova V.V., Sergeeva E.A., Shabanov D.V., Shakhova N.M., Zagainova E.V., in *Coherent-Domain Optical Methods Biomedical Diagnostics, Environmental and Material Science* (Kluwer Acad. Publ., 2004) pp 345–363.
6. Rolland J.P., Meemon P., Murali S., Thompson K.P., Lee K. *Opt. Express*, **18** (4), 3632 (2010).
7. Villiger M., Pache C., Lasser T. *Opt. Lett*., **35**, 3489 (2010).
8. Ralston T.S., Marks D.L., Carney P.S., Boppart S.A. *J. Opt. Soc. Am. A*, **23**, 1027 (2006).
9. Yu L., Rao B., Zhang J., Su J., Wang Q., Guo S., Chen Z. *Opt. Express*, **15** (12), 7634 (2007).
10. Yasuno Y., Sugisaka J., Sando Y., Nakamura Y., Makita S., Itoh M., Yatagai T. *Opt. Express*, **14** (3), 1006 (2006).
11. Yu L., Chen Z. *Opt. Lett*., **32** (20), 3005 (2007).
12. Zverev V.A. *Radiooptika* (Radiooptics) (Moscow: Sov. Radio, 1975).
13. Grebenyuk A.A., Ryabukho V.P. *Opt. Lett*., **37** (13), 2529 (2012).
14. Shabanov D.V., Gelikonov G.V., Gelikonov V.M. *Laser Phys. Lett*., **6** (10), 753 (2009).
15. Kim M.K. *Opt Lett*., **24** (23), 1693 (1999).
16. Vergnole S., Lévesque D., Lamouche G. *Opt. Express*, **18** (10), 10446 (2010).
17. Hillmann D., Huttmann G., Koch P., in *Optical Coherence Tomography and Coherence Techniques IV* (Munich, Germany: SPIE, 2009).
18. Moiseev A.A., Gelikonov G.V., Shilyagin P.A., Gelikonov V.M. *Izv. Vyssh. Uchebn. Zaved., Ser. Radiofiz*., **55** (10–11), 727 (2012).
19. Jia Y., Bagnaninchi P.O., Yang Y., Haj A.E., Hinds M.T., Kirkpatrick, S.J., Wang R.K. *J. Biomed. Opt*., **14** (3), 034014 (2009).
20. Choma M.A., Ellerbee A.K., Yang C., Creazzo T.L., Izatt J.A. *Opt. Lett*., **30** (10), 1162 (2005).
21. De Boer J.F., Milner T.E., van Gemert M.J.C., Nelson J.S. *Opt. Lett*., **22** (12), 934 (1997).
22. Tomlins P.H., Wang R.K. *Meas. Sci. Technol*., **18** (11), 3365 (2007).
23. Adler D., Ko T., Herz P., Fujimoto J.G. *Opt. Express*, **12** (22), 5487 (2004).
24. Lee J., Srinivasan V., Radhakrishnan H., Boas D.A. *Opt. Express*, **19** (22), 21258 (2011).
25. Yun S.H., Tearney G.J., de Boer J.F., Bouma B.E. *Opt. Express*, **12** (13), 2977 (2004).
26. Yang C., Wax A., Hahn M.S., Badizadegan K., Dasari R.R., Feld M.S. *Opt. Lett*., **26** (16), 1271 (2001).
27. Wang R.K. *Appl. Phys. Lett*., **90** (5), 054103 (2007).
28. Gelikonov V.M., Gelikonov G.V., Kasatkina I.V., Terpelov D.A., Shilyagin P.A. *Opt. Spektrosk*., **106** (6), 895 (2009).
29. Ghiglia D.C., Romero L.A. *Opt. Lett*., **14** (20), 1107 (1989).
30. Bamler R., Adam N., Davidson G.W., Just D. *Geosci. Remote Sensing, IEEE Trans. Image Proc*., **36** (3), 913 (1998).